Supplementary Information

Superalloys fracture process inference based on overlap analysis of 3D models

Xuecheng Zhang[1,2†], Guanghao Guo[3†], Zixin Li[1,2], Wenchao Meng[1*], Yuefei Zhang[3*], Qing Ye[1], Jin Wang[3], Shibo He[1], Xinbao Zhao[3], Jiming Chen[1], Ze Zhang[3]

[1]State Key Laboratory of Industrial Control Technology, College of Control Science and Engineering, Zhejiang University, Hangzhou, 310027, China.
[2]Polytechnic Institute, Zhejiang University, Hangzhou, 310015, China.
[3]Institute of Superalloys Science and Technology, School of Materials Science and Engineering, Zhejiang University, Hangzhou, 310027, China.

*Corresponding author(s). E-mail(s): wmengzju@zju.edu.cn; yfzhang76@zju.edu.cn;
Contributing authors: zhangxuecheng@zju.edu.cn; guogh@zju.edu.cn; lizixin@zju.edu.cn; qye@zju.edu.cn; wangjinmse@zju.edu.cn; s18he@zju.edu.cn; superalloys@zju.edu.cn; cjm@zju.edu.cn; zezhang@zju.edu.cn;
†These authors contributed equally to this work.

1 Description of in situ tensile experiments

1.1 Specimen preparation

Three sets of in situ tensile experiments and one set of ex situ tensile experiment were conducted to address specific issues. In order to clearly address these problems, two different materials were chosen for the experiments, i.e. IN718 and a new Ni-based wrought superalloy (NWS). The in situ tensile specimens(IN718 and NWS) were designed in a dog-bone shape with a unique structure to enable easy observation during the experiments. The ex situ tensile specimen(IN718) was designed as a columnar bar type with a circular cross-section(CCS). The detailed dimensions and structure of these specimens can be seen in Supplementary Figure 1 and Supplementary Figure 2.

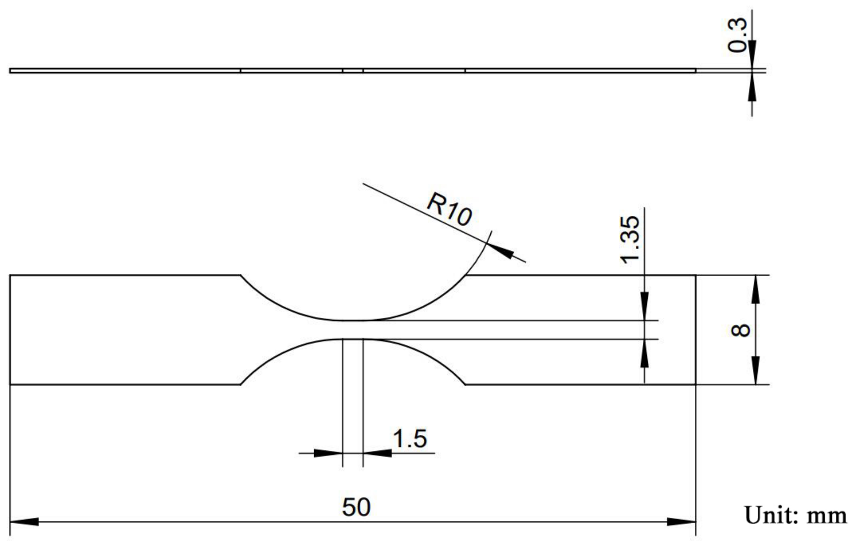

Supplementary Figure 1 Dimensions of the in situ tensile specimen.

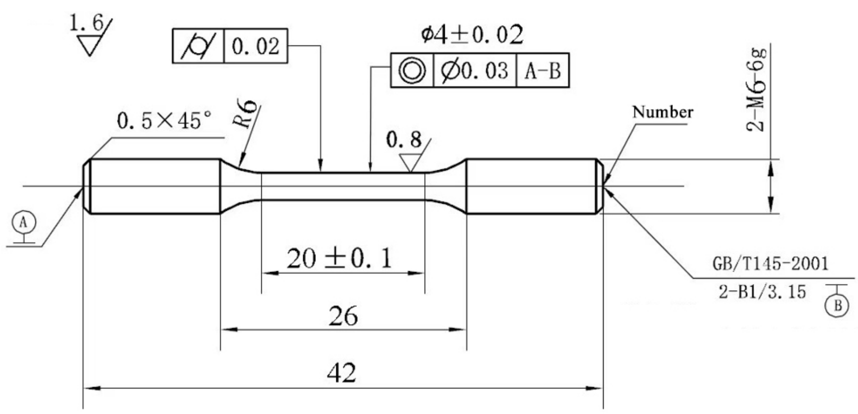

Supplementary Figure 2 Dimensions of the ex situ tensile circular cross-section specimen.

The IN718 alloy, a 30mm-diameter hot-rolled rod, had its nominal chemical composition displayed in Supplementary Table 1. The IN718 rod underwent a conventional high-strength heat treatment process. Solution annealing took place for 1h at 1050°C, followed by subsequent air cooling to room temperature. Subsequently, the solution-annealed samples experienced a two-step aging process: initial retention at 720°C for 8h, followed by furnace cooling to 620°C and holding for an additional 8h, before final air cooling to room temperature.

Additionally, the nominal chemical composition of the NWS material is displayed in Supplementary Table 2.

Supplementary Table 1 Chemical compositions of IN718 alloy (wt%)

C	Si	Mn	Cr	Fe	Mo	V	W	Co	Nb	Al	Ti	Ni
0.029	0.038	0.012	18.89	18.75	3.1	0.047	0.01	0.045	5.03	0.55	1.02	Bal.

Supplementary Table 2 Chemical compositions of NWS alloy (wt%)

Element	Fe+Co	Cr	W+Mo	Ti+Al	C+B+Zr	Ni
Weight percentage	12	16	9	3.5	0.08	Bal.

The NWS material is subjected to a two-step solution heat treatment (1120°C for 1.5h and 1050°C for 2h) to obtain the desired grain size and adjust the grain boundary microstructure, followed by a two-step aging treatment (650°C for 12h and 840°C for 4h) to control the intracrystalline microstructure, primarily the morphology and size of $\gamma^{'}$ precipitates. While the first solution treatment is followed by water cooling, all subsequent heat treatments are followed by air cooling.

Before performing the in situ tensile experiments, the samples must undergo classical metallographic preparation to eliminate the surface oxide layer and stress layer resulting from wire electrical discharge machining. The specific grinding and polishing procedures have been extensively discussed in previous studies. To effectively observe the microstructural changes during the in-situ tensile processes, a corrosion treatment is required. The corrosive solutions used for the two materials are as follows: (1) IN718: 5mL $CuCl_2$ + 100mL HCl + 100mL ethanol; (2) NWS: 2.5mL HNO_3 + 12.5mL HCl + 17mL glycerol.

1.2 In situ tensile equipment

A self-developed micro elevated-temperature tensile stage system was applied in the experiments, which mainly consists of a tensile stage for precise measurement and a heater for heating the sample to the target temperature. The concrete figure and the schematic cross-section of the working parts of the experimental equipment are shown in Supplementary Figure 3 and Supplementary Figure 4 respectively.

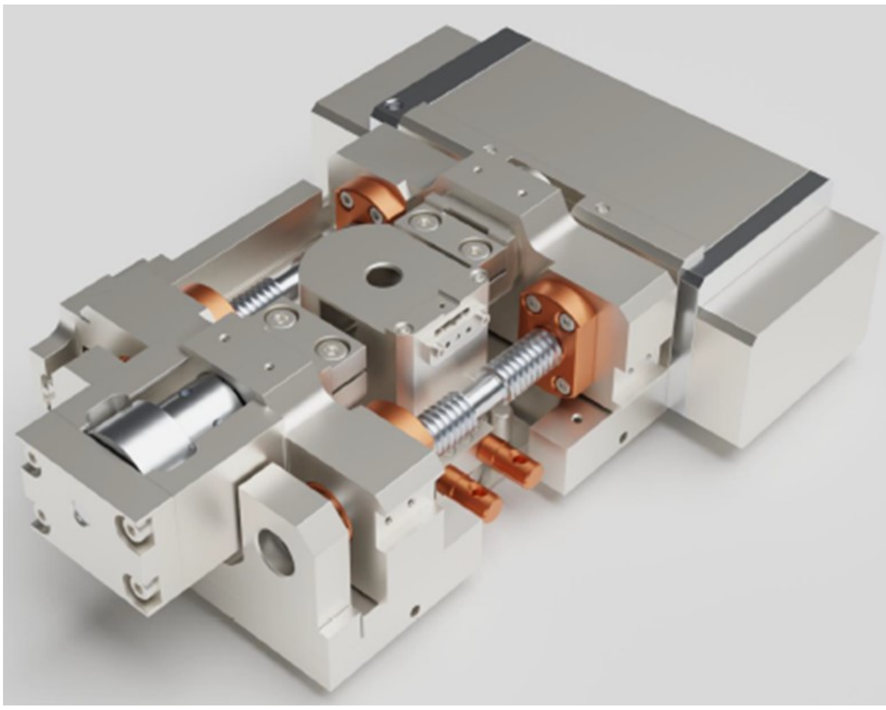

Supplementary Figure 3 The self-developed micro in situ elevated-temperature tensile stage.

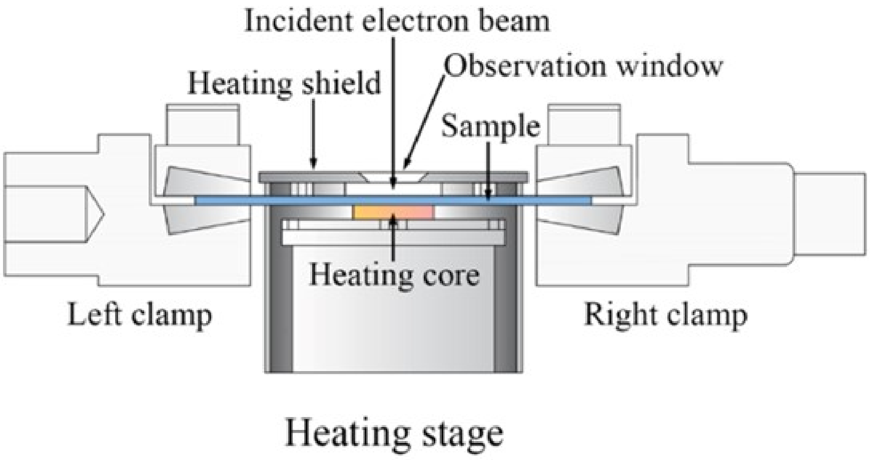

Supplementary Figure 4 The schematic cross-section of the working parts of the in situ tensile test with heating.

2 An optimized method for acquiring SEM images for 3D reconstruction

An optimized method for acquiring images is presented in Supplementary Figure 5a. In the overlooking condition, the fracture's section approximates a rectangle. For the sake of subsequent description, we define the X-axis direction as the long side direction and the Y-axis direction as the short side direction. Firstly, since the superalloy section has complex undulations, the image acquisition method is shifted from a rotating sample stage to a tilted sample stage. This prevents redundant data and limitations that arise from the high slope of the surface's undulation structure. As a result, it provides more comprehensive depth information. Secondly, we identify the specific tilt method since the area of interest is the section and its connection with the four side faces. Our method employs zero tilt as the base and uses large-scale symmetrical tilting along the X and Y axes to acquire image information of five faces and four connection points. The 45° and 135° directions with respect to the X-axis can provide additional information about the connection points between the four side faces. However, they are not the main focus of this research. Therefore, to improve the efficiency of image acquisition, we opted not to tilt in these two directions.

Given the premise of balancing reconstruction effectiveness and collection efficiency, through experimental analysis, we have identified the optimal image acquisition scheme for reconstructing the fracture of the specimen in this paper. The specimen is first fixed on an SEM sample stage, the incline angle is set to zero, and the tilt and field of view are adjusted for focusing, ensuring that the specimen section is clear and centered in the field of view. Next, execute each step in the following orders:

1. Control the sample stage to tilt 30° in the negative direction around the X-axis.
2. Control the sample stage to tilt around the X-axis in steps of 5° from -30° to 30°. Adjust the field of view and clarity at each step to obtain clear SE images.
3. Return the tilting angle of the sample stage to zero.
4. Control the sample stage to tilt 30° in the negative direction around the Y-axis.
5. Control the sample stage to tilt around the Y-axis in steps of 5° from -30° to 30°. Adjust the field of view and clarity at each step to obtain clear SE images.
6. Return the tilting angle of the sample stage to zero, and the image acquisition is complete.

A total of 25 images with a resolution of 2048 x 1024 pixels were acquired at a scan rate of 4 (3.2 μm/pixel) and saved in TIF format, cropped to remove redundant information using Photoshop, and saved in JPG format. During the entire image acquisition process, Supplementary Figure 5b displays the relative positions of the detector and the specimen. Each blue region represents the position of the detector, and the specimen is a semi-section that has been subjected to a tensile test resulting in a fracture. The acquisition of the 3D model was achieved by processing the image sequence using Agisoft Metashape software(v1.8.4) to complete the reconstruction process. Reconstruction parameters use the default settings in the software.

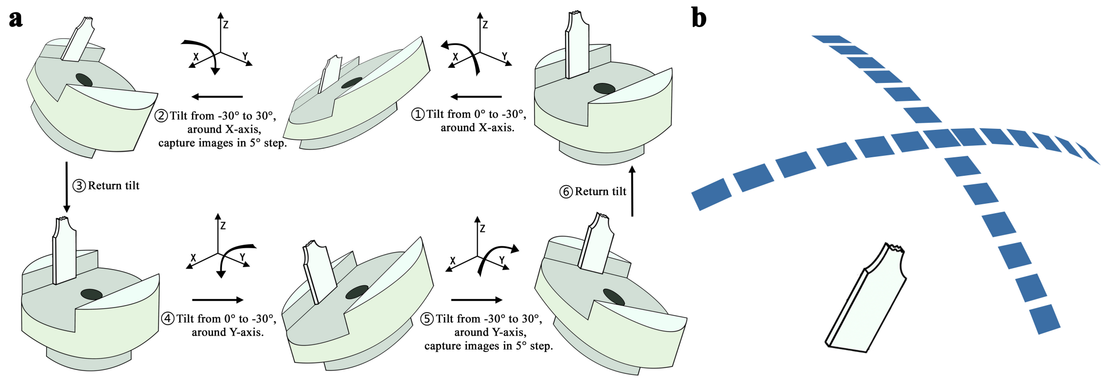

Supplementary Figure 5 Optimized scheme for original image acquisition. **a** Detailed tilting steps of the sample stage. **b** Relative positions relationship between detector and specimen.

3 Data for scale calibration

Taking Fracture A as an example, two marked points with distinctive features are sought in the cross section of Supplementary Figure 6a. The height Z of the sample stage was adjusted to capture a consecutive series of images. This procedure allows us to capture a sequence of images that exhibit an increasing and subsequently decreasing level of sharpness, as depicted in Supplementary Figure 6b. The score curve of the image sequence, evaluated using the normalized variance equation, is presented in Supplementary Figure 6c.

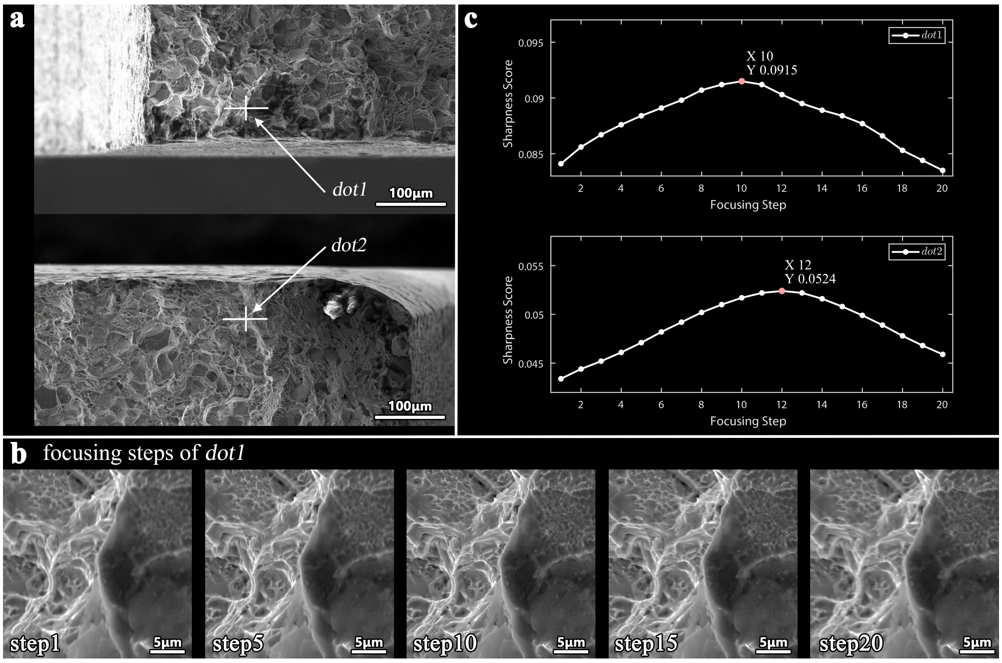

Supplementary Figure 6 Scale calibration based on image sharpness evaluation (Fracture A). **a** Two marking dots with distinct features. **b** Some typical images from the focusing steps of *dot1*. **c** Sharpness score curves of the image sequences of two marking dots.

As a complement, Supplementary Figure 7 shows the score curves for a total of four fracture models for both sets of experiments for alloy IN718 at scale calibration.

4 Inference method of fracture process

4.1 Specific implementation programme

Using the results of HT fracture process inference as an illustrative example, we describe the specific implementation programme of the inference method. Firstly, the corresponding fracture

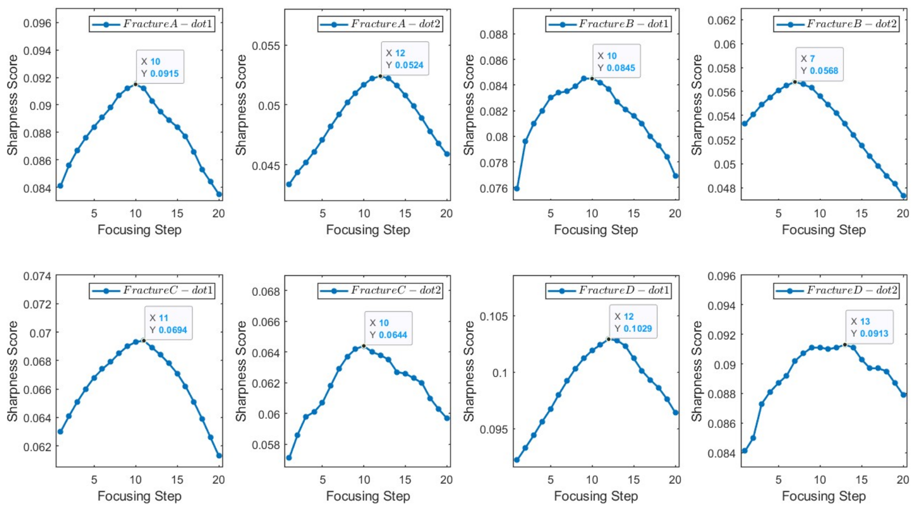

Supplementary Figure 7 Image sharpness assessment curves for four fracture models in scale calibration sessions.

models are gradually brought together until they overlap entirely, as demonstrated in Supplementary Figure 8a. To observe the projection of the target fracture surface coinciding with the opposite fracture surface, it can be observed from inside the opposite fracture. The complete morphology of the target fracture surface can be seen when two fracture models are fully overlapped, as Supplementary Figure 8d depicts. This stage signifies the connected state of the specimen during the actual tensile process prior to fracture initiation. Subsequently, a gradual distancing from the associated model occurs with a step size of 20μm, as illustrated in Supplementary Figure 8b. During the tensile process, the region where cracking initiates displays a notch in the figure due to its reduced elongation rate, depicted by the black area within the black circle in Supplementary Figure 8e. With the increasing separation of the corresponding model, the cracking process, encompassing crack initiation, propagation, and ultimate fracture, becomes evident. In Supplementary Figure 8c, only the region within the black circle exhibits overlapping between the corresponding models, indicating the location of the fracture termination, as seen in Supplementary Figure 8f. The labeled distances in the figure represent the displacement at which the corresponding model gradually moves away, equivalent to the tensile displacement observed in actual tensile experiments.

4.2 Methodological soundness validation

To further validate the accuracy and effectiveness of the tensile fracture process inference, we conducted additional analyses using in situ tensile experiments conducted on NWS specimens at RT. Supplementary Figure 9a illustrates the five typical stages of the fracture process inference results. Supplementary Figure 9b displays the result following complete specimen fracture, indicating specific observed areas and perspectives marked with $'\oplus'$ and $'\ominus'$. The data presented in Supplementary Figure 9c is derived from in situ tensile experiments, showcasing the evolution of surface morphology during the stretching process. The material's fracture process becomes increasingly apparent as the deformation progresses. The position of the initial surface cracking coincides with the region highlighted by the white arrow in Supplementary Figure 9a, thereby providing robust evidence for the highly accurate fracture process inferred by our framework.

4.3 Methodological applicability validation

Furthermore, we employed our proposed methodology to reconstruct and analyze the ex situ tensile fractures of circular cross-section specimens made of IN718 to validate the method's universality. Supplementary Figure 10a delineates six typical stages of the inferred fracture process. In Supplementary Figure 10b, the original SEM images of the fractures are depicted, revealing the fundamental characteristics of the morphology; however, they lack precise 3D perspective and quantitative analysis. Subsequently, Supplementary Figure 10c showcases the

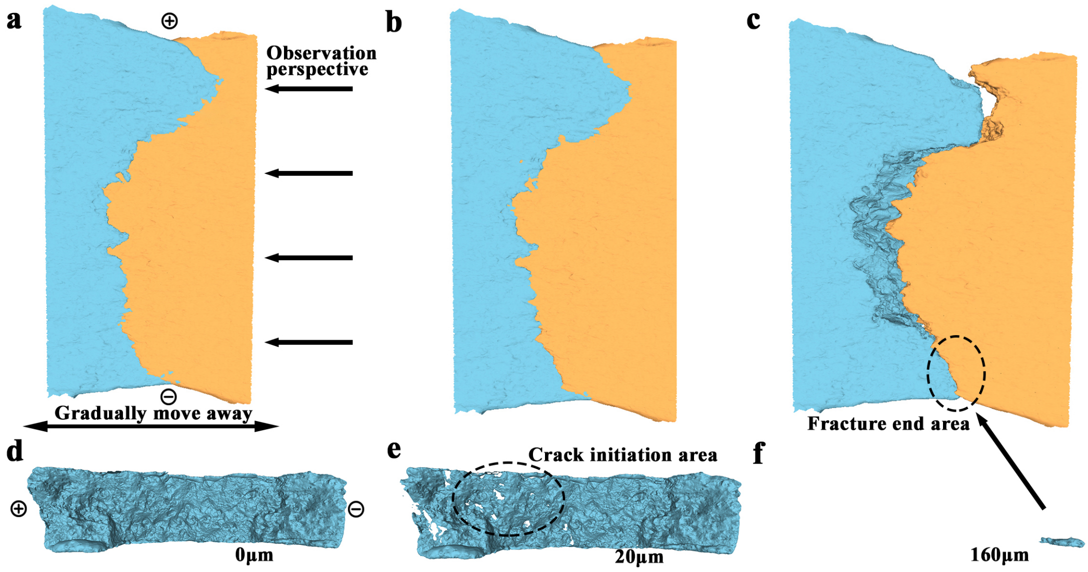

Supplementary Figure 8 The implementation process of 3D models overlap analysis. **a** A pair of completely overlapping fracture models, with the direction indicated by the arrow representing the observation direction. **b** Two models gradually separate, with a displacement interval of 20μm. **c** Two models progressively move away from each other, approaching the point of separation. **d** Observation results when completely overlapped. **e** Observation results at a displacement of 20μm, at which point the region with already developed cracks can be observed within the fracture surface. **f** Observation results at a displacement of 160μm reveal the residual area that aligns with the fracture end area in **c**.

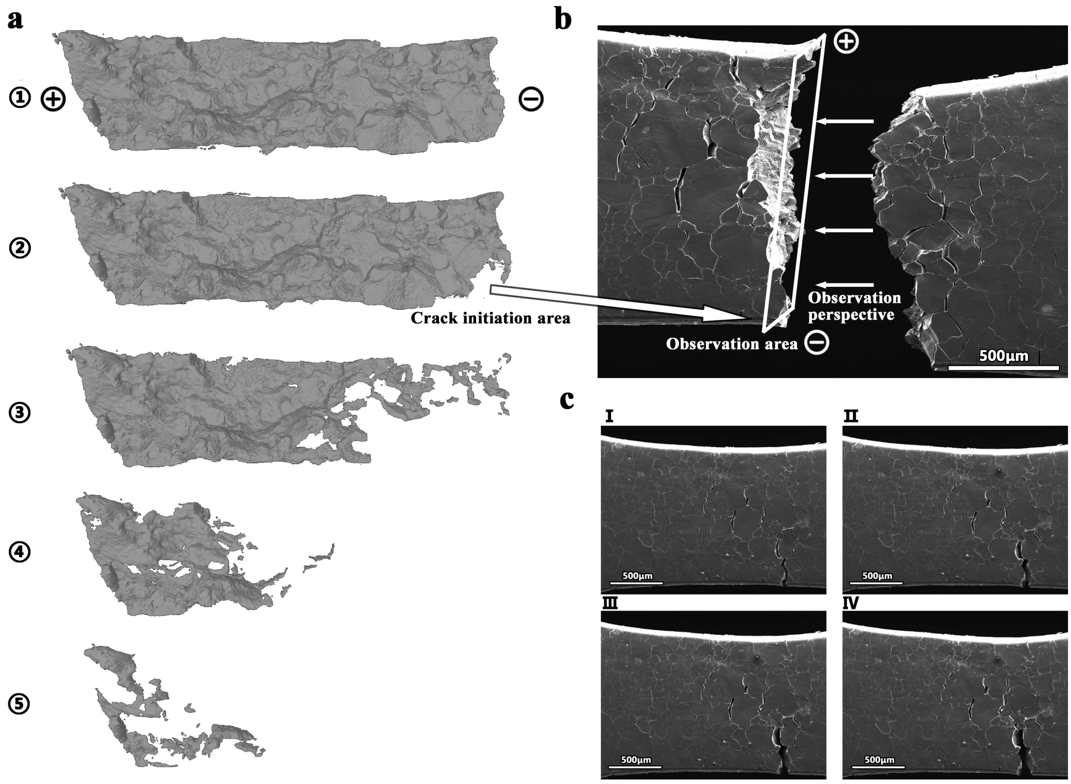

Supplementary Figure 9 Methodological soundness validation of 3D model overlap analysis. **a** The fracture process inference result of in situ RT tensile experiment fracture surface of NWS. **b** SEM image of the specimen after fracture, with labels indicating the observation perspective and area. **c** The crack propagation in the in situ tensile experiment.

results of the 3D reconstruction and registration of the fractures. A comparative study with Supplementary Figure 10b demonstrates the practical application of our methodology to circular section specimens' fractures, thereby affirming the universality of our framework.

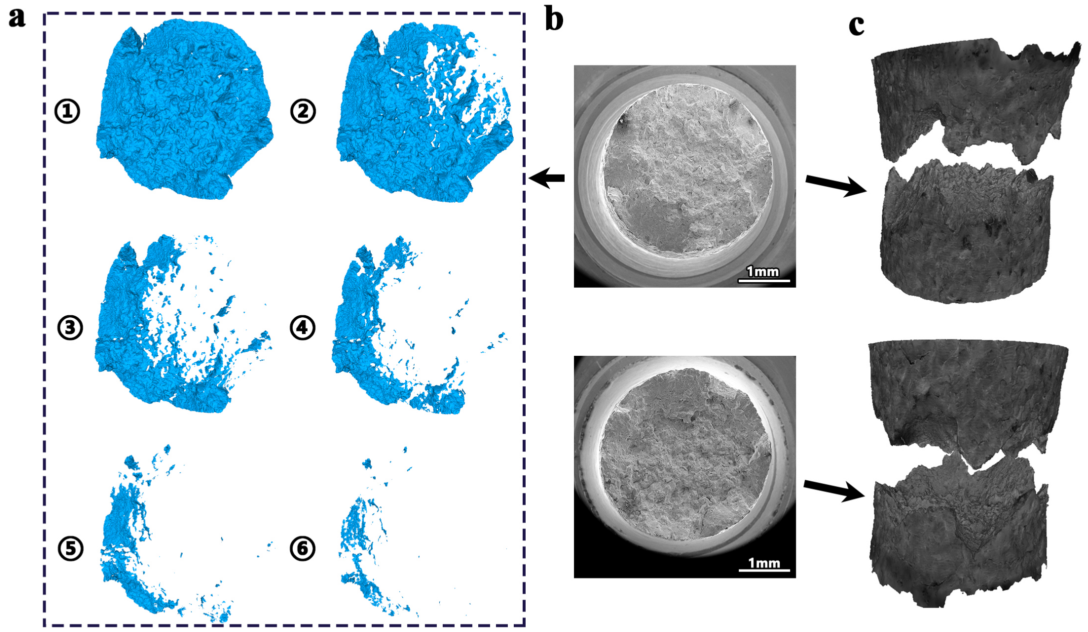

Supplementary Figure 10 Methodological applicability validation of 3D model overlap analysis on a circular cross-section specimen. **a** The fracture process inference result of ex situ RT tensile experiment fracture surface of CCS. **b** SEM image of the specimen's fractures. **c** 3D fracture morphology models of CCS.